CrossMark

# Reduction of Oxide Mixtures of (Fe$_2$O$_3$ + CuO) and (Fe$_2$O$_3$ + Co$_3$O$_4$) by Low-Temperature Hydrogen Plasma

K. C. Sabat[1,2] · R. K. Paramguru[1,2] · B. K. Mishra[1]

**Abstract** The paper presents experimental results pertaining to the reduction of oxide mixtures namely (Fe$_2$O$_3$ + CuO) and (Fe$_2$O$_3$ + Co$_3$O$_4$), by low-temperature hydrogen plasma in a microwave hydrogen plasma set-up, at microwave power 750 W and hydrogen flow rate $2.5 \times 10^{-6}$ m$^3$ s$^{-1}$. The objective was to examine the effect of addition of CuO or Co$_3$O$_4$, on the reduction of Fe$_2$O$_3$. In the case of the Fe$_2$O$_3$ and CuO mixture, oxides were reduced to form Fe and Cu metals. Enhancement of reduction of iron oxide was marginal. However, in the case of the Fe$_2$O$_3$ and Co$_3$O$_4$ mixture, FeCo alloy was formed within compositions of Fe$_{70}$Co$_{30}$, to Fe$_{30}$Co$_{70}$. Since the temperature was below 841 K, no FeO formed during reduction and the sequence of Fe$_2$O$_3$ reduction was found to be Fe$_2$O$_3$ → Fe$_3$O$_4$ → Fe. Reduction of Co$_3$O$_4$ preceded that of Fe$_2$O$_3$. In the beginning, the reduction of oxides led to the formation of Fe–Co alloy that was rich in Co. Later Fe continued to enter into the alloy phase through diffusion and homogenization. The lattice strain of the alloy as a function of its composition was measured. In the oxide mixture in which excessive amount of Co$_3$O$_4$ was present, all the Co formed after reduction could not form the alloy and part of it appeared as FCC Co metal. The crystallite size of the alloy was in the range of 22–30 nm. The crystal size of the Fe–Co alloy reduced with an increase in Co concentration.

**Keywords** Reduction of oxide mixtures · Reduction of cupric oxide · Reduction of iron oxide · Reduction of cobalt oxide · Low-temperature hydrogen plasma · FeCo alloy
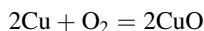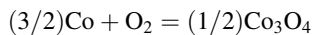
✉ B. K. Mishra
bkm.immt@gmail.com

1   CSIR-Institute of Minerals and Materials Technology, Bhubaneswar 751013, India

2   KIIT University, Bhubaneswar 751024, India

✦ Springer

## Introduction

Recently, reduction of metal oxides by hydrogen plasma has been extensively reviewed [1], and some studies were made on low-temperature hydrogen plasma for reduction of iron oxide [2–4], cobalt oxide [5] and copper oxide [6]. In all these cases, successful reduction took place with the decrease in activation energy due to the presence of activated species in hydrogen plasma. Another important point was that the equilibrium partial pressure of atomic hydrogen needed to reduce these oxides goes down at lower temperatures unlike that for the reduction with molecular hydrogen; thus low-temperature operations are favorable for reduction with hydrogen plasma. Further, the free energy change for reduction reactions of oxides with these excited species becomes more favorable. In these contexts, the reduction of metal oxide mixtures assumes significance. For example, reduction of an oxide, say oxide-1, placed in the Ellingham diagram with free energy change $\Delta G_1^0$, depends on the difference between this free energy and that of the reductant ($\Delta G_r^0$). First of all, when this difference $\{(\Delta G_r^0) - \Delta G_1^0\}$ is negative the reaction proceeds in the forward direction and secondly, the magnitude of this difference is an indicator of the driving force for the reduction reaction. Similarly, for a second oxide ($\Delta G_2^0$), the difference $\{(\Delta G_r^0) - \Delta G_2^0\}$ is significant for its reduction. When these two oxides are reduced together, then the effective energy difference is somewhere between $\{(\Delta G_r^0) - \Delta G_1^0\}$ and $\{(\Delta G_r^0) - \Delta G_2^0\}$. Thus, there is a possibility that reduction of the oxide with lower difference against the reductant may get the advantage of the extra energy available from the other oxide. Again, in the case of good miscibility between the two metals, coming out as the reduction reaction product and forming an alloy, there would be a further advantage on energy count. Therefore, reduction of oxide mixtures has been chosen as the topic for this study. Based on the successful reduction of the three oxides, $Fe_2O_3$, $CuO$, and $Co_3O_4$, the binary mixtures of ($Fe_2O_3$ + $CuO$) and ($Fe_2O_3$ + $Co_3O_4$) have been selected for this study.

At first, the thermodynamic feasibility of all the reactions pertaining to the oxide mixtures through estimation of Gibbs free energy change at various temperatures (Ellingham diagram) is evaluated (Fig. 1). For each oxide, wherever sub-oxides were available, one composite reaction is considered as described in the following lines:

$$6CoO + O_2 = 2Co_3O_4 \tag{1.1}$$

$$3[2Co + O_2 = 2CoO] \tag{1.2}$$

$$6Co + 4O_2 = 2Co_3O_4$$
$$\text{Or,} \tag{1}$$
$$(3/2)Co + O_2 = (1/2)Co_3O_4$$

$$2Cu_2O + O_2 = 4CuO \tag{2.1}$$

$$4Cu + O_2 = 2Cu_2O \tag{2.2}$$

$$4Cu + 2O_2 = 4CuO$$
$$\text{Or,} \tag{2}$$
$$2Cu + O_2 = 2CuO$$
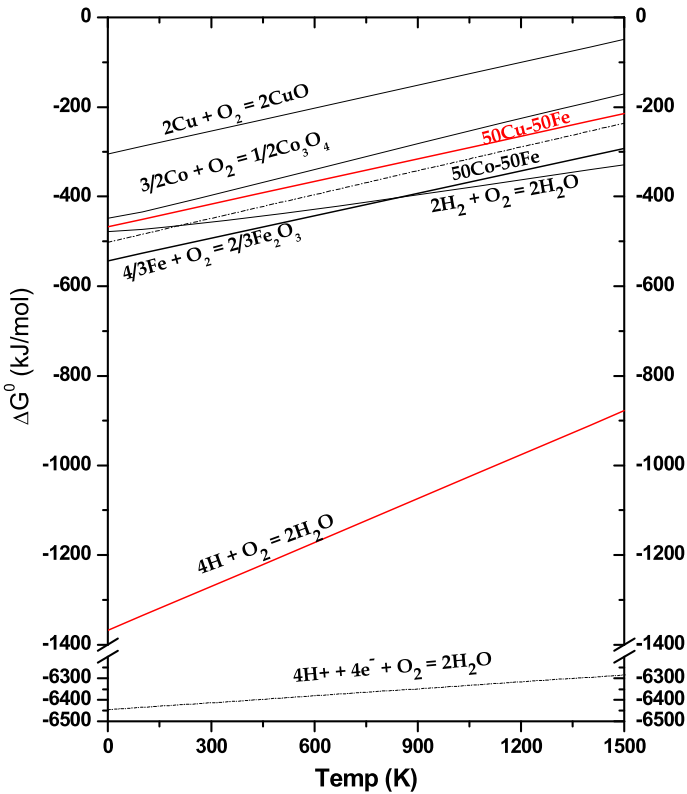
**Fig. 1** Ellingham diagram for different metal oxide systems

$$4Fe_3O_4 + O_2 = 6Fe_2O_3 \tag{3.1}$$

$$2[6FeO + O_2 = 2Fe_3O_4] \tag{3.2}$$

$$6[2Fe + O_2 = 2FeO] \tag{3.3}$$

$$12Fe + 3O_2 = 6Fe_2O_3$$
$$\text{Or,} \tag{3}$$
$$4Fe + O_2 = 2Fe_2O_3$$

$$2H_2 + O_2 = 2H_2O \tag{4}$$

$$4H + O_2 = 2H_2O \tag{5}$$

$$4(H^+ + e^-) + O_2 = 2H_2O \tag{6}$$
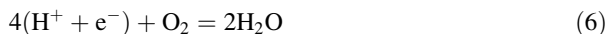
The Figure (Fig. 1) shows copper oxide at the top followed by cobalt oxide and iron oxide. Hydrogen lines come next. The $H_2$ line is practically intersecting the iron oxide line. Obviously, the difference in $\Delta G^0$ between the lines for copper oxide and hydrogen is the largest and therefore, it is expected that copper oxide would be reduced easily with hydrogen. Similarly, the difference in $\Delta G^0$ between the iron oxide and hydrogen lines is the

lowest amongst these oxides, and it would be relatively difficult to reduce iron oxide by hydrogen. The previous publications [1–6] confirm this aspect. When iron oxide and copper oxide are mixed in proportions corresponding to a particular ratio of iron and copper (say 50:50), and the Gibbs free energy line for this mixture would appear somewhere in between the lines for copper and iron oxides. Hence, the difference in $\Delta G^0$ between this line and the hydrogen line would be higher than that between the iron oxide and hydrogen lines. Further, in case the two metals form an alloy and add negative free energy, reduction of iron oxide by hydrogen from this mixture is expected to be better than when it is reduced individually. Similar results may be expected from oxide mixtures of iron and cobalt.

It is important to examine the possibility of alloy formation between Fe–Cu and Fe–Co, the metal couples coming out as reaction products from the reduction of binary oxide couples $Fe_2O_3$–CuO and $Fe_2O_3$–$Co_3O_4$, respectively.

*Fe-Cu* In the equilibrium state, they do not obey the Hume-Rothery rules of extensive solid solubility. So, they don't form extensive solid solutions. However, Fe and Cu have very little mutual solid solubility and form no inter-metallic compounds [7]. Interestingly, polycrystalline or amorphous metastable FeCu solid solution can be formed in non-equilibrium processes, like rapid quenching techniques (vapor-quenching/high rate sputtering) or by high energy ball milling [7, 8]. In these cases, either Cu-rich FCC phase (paramagnetic) or Fe-rich BCC phase (ferromagnetic) may result. Even a particular composition like $Fe_{50}Cu_{50}$ can be grown as a single crystalline ordered alloy by means of epitaxially stacking mono-layers of Fe and Cu alternately unto an appropriate substrate following sophisticated growth techniques like pulsed-laser deposition [7].

*Fe–Co* Iron and Cobalt obey the Hume-Rothery rules of extensive solid solubility. So they form substitutional solid solutions. The Fe–Co alloys occupy an important position because of their unique magnetic properties such as high Curie temperatures, the highest saturation magnetizations, high permeability, low losses and relative strength [9, 10]. Near-equiatomic FeCo alloys are BCC at low temperature, and FCC at a temperature above ~1256 K. The BCC phase undergoes ordering to a B2 (CsCl) structure at temperatures below ~1003 K.

Based on the facts and figures described above, the choice of the two mixtures ($Fe_2O_3$–CuO and $Fe_2O_3$–$Co_3O_4$) in this study may fall into two categories: (1) the first one may not produce an alloy barring some interesting phenomenon from low-temperature hydrogen plasma system, and (2) the second one may form an alloy. The composition of the oxide mixtures in the present study are selected: (a) a mixture of CuO and $Fe_2O_3$ in such a proportion which would result in a metallic mixture 50%Cu–50%Fe, when totally reduced, (b) mixtures of $Co_3O_4$ and $Fe_2O_3$ in three proportions such that the resultant product when totally reduced would be Co–Fe in the following proportions: (30:70), (50:50) and (70:30).

## Experimental Details

The experimental details pertaining to the raw materials, preparation of compacted hematite pellets, the experimental set-up, procedure for experiments and material (raw material and products) characterization are presented in the earlier reports [5, 6]. In the current investigation, the transition metal oxides e.g. copper oxide, cobalt oxide, and iron oxide were used. The oxides used were of chemical grade; which were used in pellet form during reduction.

The microwave plasma reactor supplied by IMAT Pvt. Ltd., India, which incorporates a 6000 W at $2.45 \times 10^9$ s$^{-1}$ microwave generator to produce plasma at high power densities. The high-frequency electromagnetic waves interact with the supplied hydrogen gas to produce the hydrogen plasma. The sample on a molybdenum sample holder is placed at the center of the reaction chamber within the plasma range. The temperature, pressure, hydrogen flow rate, etc., are properly monitored all through. An X'Pert PRO-PANalytical model no. 3040160 was used for X-ray diffraction (XRD) studies of the phases in the reduced samples. The quantitative estimation of the progress of the reaction was made by incorporating weight loss data along with the phase analysis.

## Results and Discussion

### The Mixture of Iron Oxide and Copper Oxide

A set of experiments was conducted with hydrogen plasma at a microwave power of 750 W and hydrogen flow rate of $2.5 \times 10^{-6}$ m$^3$ s$^{-1}$ to reduce a mixture of CuO and Fe$_2$O$_3$ in such a proportion which would result in a metallic mixture of 50%Cu + 50%Fe, when totally reduced. The results of weight loss at various time periods along with pressure and temperature values are reported in Table 1. The reduction rate plots are shown in Fig. 2, and the XRD results are shown in Fig. 3. For the sake of comparison, the results of reduction of CuO and Fe$_2$O$_3$ individually at identical conditions were also reported. The results show that the reduction level is lower for iron oxide (52% by 3600 s with hydrogen utilization of just 6.0%), higher for CuO (~95% by 900 s with hydrogen utilization of 28.8%) and intermediate for the mixture (together 93% by 3600 s with 9.43% hydrogen utilization). This trend is according to the free energy difference between the oxide and the

**Table 1** Weight loss as well as maximum pressure and temperature for reduction of Fe$_2$O$_3$, CuO and (Fe$_2$O$_3$ + CuO) with hydrogen plasma. Microwave power: 750 W and hydrogen flow rate: $2.5 \times 10^{-6}$ m$^3$ s$^{-1}$

| Raw material | Time/s | $T_{max}$,/K | $P_{max}$,/$10^2$ Pa | Initial wt/ $10^{-3}$ kg | Final wt/ $10^{-3}$ kg | Wt loss,/ $10^{-3}$ kg | Reduction, in % |
|---|---|---|---|---|---|---|---|
| Fe$_2$O$_3$ | 300 | 816.2 | 1.508 | 2.528 | 2.401 | 0.127 | 16.7 |
| Fe$_2$O$_3$ | 600 | 860.9 | 1.575 | 2.535 | 2.362 | 0.173 | 22.7 |
| Fe$_2$O$_3$ | 900 | 807.0 | 1.591 | 2.539 | 2.324 | 0.214 | 28.1 |
| Fe$_2$O$_3$ | 1800 | 816.9 | 1.724 | 2.541 | 2.232 | 0.308 | 40.4 |
| Fe$_2$O3 | 3600 | 821.1 | 1.524 | 2.461 | 2.075 | 0.385 | 52.1 |
| CuO | 300 | 761.9 | 1.967 | 2.370 | 2.279 | 0.091 | 19.1 |
| CuO | 600 | 857.4 | 2.441 | 2.430 | 2.153 | 0.276 | 56.6 |
| CuO | 900 | 903.2 | 2.591 | 2.434 | 1.971 | 0.462 | 94.5 |
| CuO | 1200 | 889.4 | 2.475 | 2.490 | 1.978 | 0.511 | 102.1 |
| CuO | 1800 | 886.8 | 2.567 | 2.433 | 1.931 | 0.501 | 102.4 |
| 50Fe-50Cu | 360 | 626.5 | 1.824 | 2.566 | 2.413 | 0.153 | 23.6 |
| 50Fe-50Cu | 900 | 881.2 | 1.708 | 2.550 | 2.188 | 0.362 | 56.2 |
| 50Fe-50Cu | 1200 | 824.4 | 1.891 | 2.551 | 2.134 | 0.417 | 64.6 |
| 50Fe-50Cu | 1800 | 824.4 | 1.891 | 2.568 | 2.093 | 0.475 | 73.2 |
| 50Fe-50Cu | 3600 | 746.2 | 2.091 | 2.555 | 1.949 | 0.605 | 93.8 |
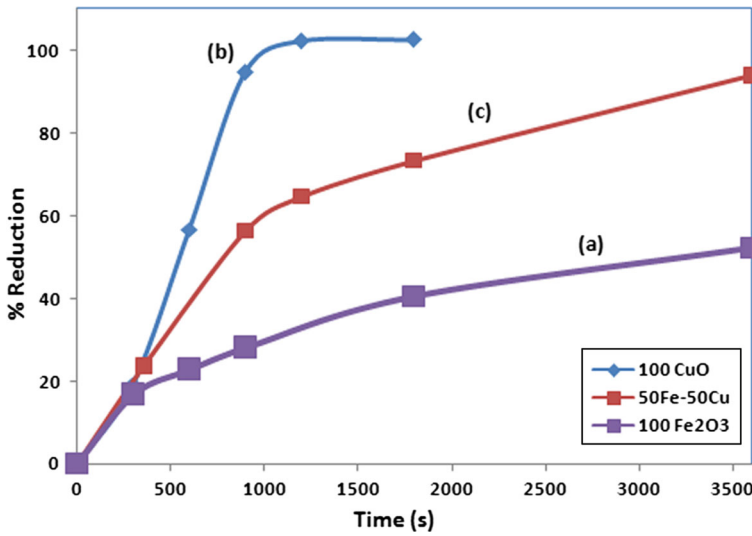
**Fig. 2** Rate plots for reduction of (*a*) 100% $Fe_2O_3$, (*b*) 100% CuO, and (*c*) 50% $Fe_2O_3$ + 50% CuO. Microwave power: 750 W and hydrogen flow rate: $2.5 \times 10^{-6}$ $m^3$ $s^{-1}$



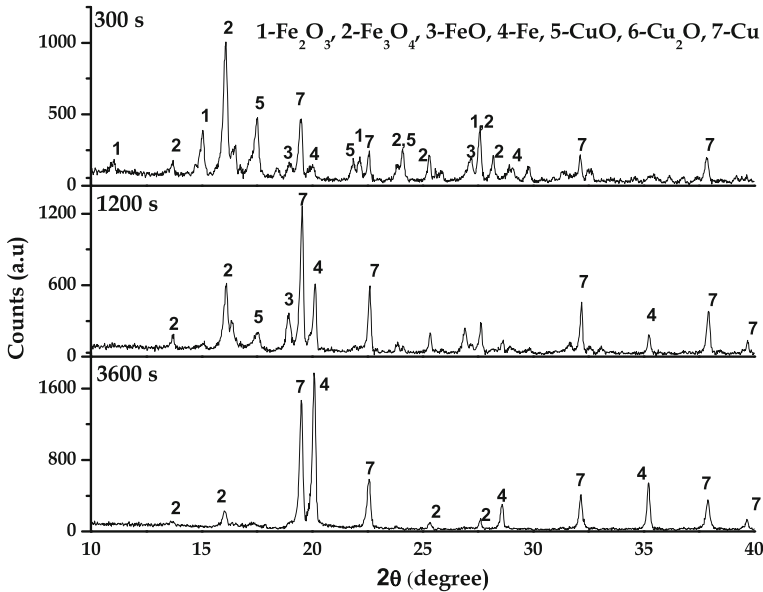**Fig. 3** XRD plots for reduction of (50% $Fe_2O_3$ + 50% CuO). Microwave power: 750 W and hydrogen flow rate: $2.5 \times 10^{-6}$ $m^3$ $s^{-1}$

reductant. Since $\{(\Delta G_r^0) - \Delta G_{Cu}^0\}$ is greater than $\{(\Delta G_r^0) - \Delta G_{Fe}^0\}$, reduction of copper oxide is faster than that of iron oxide. Figure 4 presents plots for reduction levels (at various time periods: 300, 900, 1800, and 3600 s) against $\{\Delta G_r^0) - \Delta G_x^0\}$, where x denotes
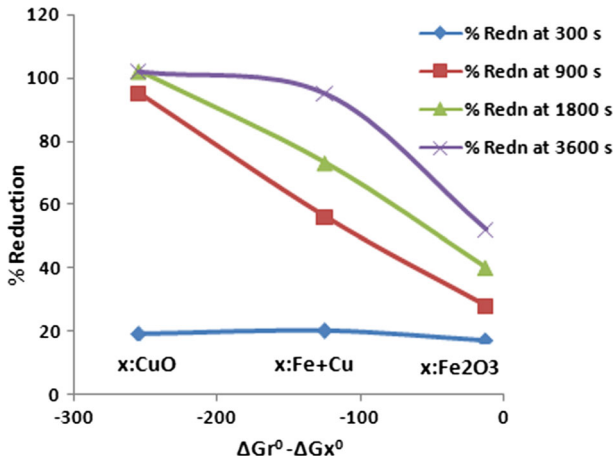
**Fig. 4** Extent of reduction (%) versus $\{(\Delta G_r^0) - \Delta G_x^0\}$. {x denotes $Fe_2O_3$, CuO and ($Fe_2O_3$, CuO)}. Microwave power: 750 W and hydrogen flow rate: $2.5 \times 10^{-6}$ m$^3$ s$^{-1}$

$Fe_2O_3$, CuO or ($Fe_2O_3$, CuO mixture). The plots follow the similar trend that is reduction is higher at higher (negative) values of $\{\Delta G_r^0\} - \Delta G_x^0\}$. The points at 300 s do not show higher copper reduction because CuO reduction encounters an induction period [6], which is observed in Fig. 2 for reduction of CuO; whereas, the same point at 300 s in Fig. 2 results in higher iron reduction since all the $Fe_2O_3$ have reduced to lower oxides by that time [2, 3]. The peaks in the XRD plots (Fig. 3 and Table 2) confirm the reduction products to be Cu (JCPDS file no: 00-004-0836) and Fe (JCPDS file no: 00-006-0696) metals. The lattice parameters of Cu and Fe metals are calculated from the XRD pattern and those found to be 3.6219 and 2.8701 Å, respectively. These values are close to their respective theoretical values of 3.6150 and 2.8670 Å. Hence, it can be concluded that the reduction of CuO and $Fe_2O_3$ continued independently, resulting in the production of their respective metals only; alloy formation was absent. Figure 2 and 3 also show that most of the CuO

**Table 2** XRD data obtained from the product after reduction of ($Fe_2O_3$ + CuO) with hydrogen plasma for 3600 s. Microwave power: 750 W and hydrogen flow rate: $2.5 \times 10^{-6}$ m$^3$ s$^{-1}$

| Serial No. | Plane h k l | Cu: JCPDS File: 00-004-0836: d[Å] (I) | Fe: JCPDS File: 00-006-0696: d[Å] (I) | Experimental product at 60′: d[Å] (I) |
|---|---|---|---|---|
| 1 | 1 1 1 | 2.08800 (100) | | 2.09475 (85) |
| 2 | 1 1 0 | | 2.02680 (100) | 2.03112 (100) |
| 3 | 2 0 0 | 1.80800 (46) | | 1.81096 (32) |
| 4 | 2 0 0 | | 1.43320 (20) | 1.43504 (14) |
| 5 | 2 2 0 | 1.27800 (20) | | 1.28018 (20) |
| 6 | 2 1 1 | | 1.17020 (30) | 1.17190 (27) |
| 7 | 3 1 1 | 1.09000 (17) | | 1.09132 (26) |
| 8 | 2 2 2 | 1.04360 (5) | | 1.04474 (6) |
| 9 | 2 2 0 | | 1.01340 (10) | 1.01524 (7) |
| 10 | 3 1 0 | | 0.90640 (12) | 0.90749 (7) |

have been reduced by 1200 s, whereas peaks of Fe metal start showing up at 360 s which grow with the rise in time. Even then a small part of iron oxide remains unreduced even at 3600 s.

## The Mixture of Iron Oxide and Cobalt Oxide

In this section, one set of reduction experiments were conducted with mixtures of $Co_3O_4$ and $Fe_2O_3$ in a proportion such that the resultant product when totally reduced would be metallic Co-Fe in a ratio of 50:50. The microwave power of 750 W and hydrogen flow rate of $2.5 \times 10^{-6}$ $m^3$ $s^{-1}$ was maintained all through the experiments. The results of weight loss at various time periods along with pressure and temperature data are reported in Table 3. The reduction rate plots are presented in Fig. 5, and the XRD results are shown in Fig. 6 and Table 4. Figure 7 shows the extent of reduction (%) versus $\{(\Delta G_r^0) - \Delta G_x^0\}$ where x denotes $Fe_2O_3$, $Co_3O_4$ or ($Fe_2O_3 + Co_3O_4$) with the specific proportion. Unlike in the case of the $CuO$-$Fe_2O_3$ mixture, here, Fig. 6, as well as Table 4, shows the Fe–Co alloy to be the dominant product with three secondary peaks of Co metal being present with intensities between 0.97 to 1.44% only. Therefore, higher levels of reduction for iron oxide

**Table 3** Weight loss as well as maximum pressure and temperature for reduction of $Fe_2O_3$, ($50Co_3O_4$ + $50Fe_2O_3$) and $Co_3O_4$ with hydrogen plasma. Microwave power: 750 W and hydrogen flow rate: $2.5 \times 10^{-6}$ $m^3$ $s^{-1}$

| Raw Material | Time/s | $T_{max}$/K | $P_{max}$/$10^2$ Pa | Initial wt/ $10^{-3}$ kg | Final wt/ $10^{-3}$ kg | Wt loss,/ $10^{-3}$ kg | Reduction, in % |
|---|---|---|---|---|---|---|---|
| $Fe_2O_3$ | 300 | 816.2 | 1.508 | 2.528 | 2.401 | 0.127 | 16.7 |
| $Fe_2O_3$ | 600 | 860.9 | 1.575 | 2.535 | 2.362 | 0.173 | 22.7 |
| $Fe_2O_3$ | 900 | 807.0 | 1.591 | 2.539 | 2.324 | 0.214 | 28.1 |
| $Fe_2O_3$ | 1800 | 816.9 | 1.724 | 2.541 | 2.232 | 0.308 | 40.4 |
| $Fe_2O_3$ | 3600 | 821.1 | 1.524 | 2.461 | 2.075 | 0.385 | 52.1 |
| 50Fe-50Co | 300 | 757.6 | 2.208 | 2.550 | 2.386 | 0.164 | 23.7 |
| 50Fe-50Co | 600 | 770.1 | 2.233 | 2.543 | 2.274 | 0.268 | 38.8 |
| 50Fe-50Co | 900 | 781.1 | 2.133 | 2.529 | 2.213 | 0.316 | 46.1 |
| 50Fe-50Co | 1200 | 783.2 | 2.241 | 2.550 | 2.092 | 0.458 | 66.3 |
| 50Fe-50Co | 1500 | 787.5 | 2.087 | 2.552 | 2.076 | 0.475 | 68.6 |
| 50Fe-50Co | 1800 | 836.3 | 2.157 | 2.553 | 2.039 | 0.514 | 74.2 |
| 50Fe-50Co | 3600 | 860.7 | 2.208 | 2.540 | 1.876 | 0.663 | 96.3 |
| $Co_3O_4$ | 120 | 595.1 | 2.600 | 2.456 | 2.377 | 0.079 | 13.3 |
| $Co_3O_4$ | 300 | 719.2 | 3.049 | 2.467 | 2.198 | 0.269 | 45.5 |
| $Co_3O_4$ | 600 | 697.3 | 2.749 | 2.510 | 2.091 | 0.418 | 70.2 |
| $Co_3O_4$ | 900 | 709.2 | 2.924 | 2.451 | 1.950 | 0.501 | 85.2 |
| $Co_3O_4$ | 1200 | 766.3 | 2.875 | 2.454 | 1.869 | 0.584 | 99.2 |
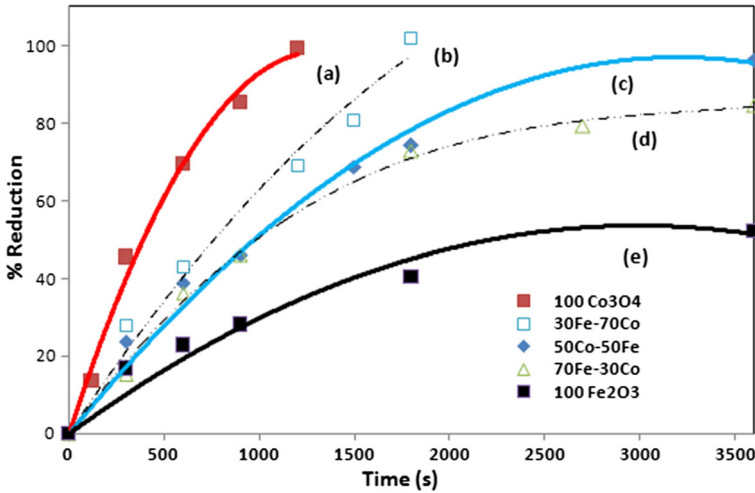
**Fig. 5** Rate plots for reduction of (*a*) 100% $Co_3O_4$, (*b*) 70% $Co_3O_4$ + 30% $Fe_2O_3$, (*c*) 50% $Fe_2O_3$ + 50% $Co_3O_4$, (*d*) 30% $Co_3O_4$ + 70% $Fe_2O_3$ and (*e*) 100% $Fe_2O_3$, Microwave power: 750 W and hydrogen flow rate: $2.5 \times 10^{-6}$ $m^3$ $s^{-1}$
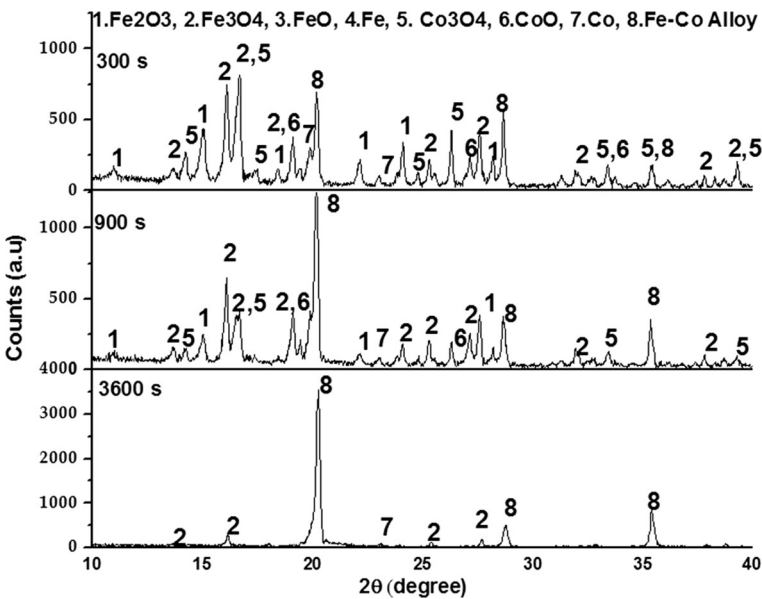


**Fig. 6** XRD plots for reduction of $Fe_2O_3$ + $Co_3O_4$ which would result in 50–50 Fe-Co metal. Microwave power: 750 W and hydrogen flow rate: $2.5 \times 10^{-6}$ $m^3$ $s^{-1}$

have been achieved when the oxide mixture is reduced in comparison to the extent of reduction when iron oxide is charged individually (Table 3 and Fig. 5). The reduction level of iron oxide was only 52% by 3600 s when it was reduced independently, which (together)

**Table 4** XRD data obtained from the product after reduction of ($50Fe_2O_3 + 50Co_3O_4$) with hydrogen plasma for 3600 s. Microwave power: 750 W and hydrogen flow rate: $2.5 \times 10^{-6}$ m$^3$ s$^{-1}$

| Serial No. | Plane h k l | Co: JCPDS File: 00-015-0806: d[Å] (I) | Co$_{50}$Fe$_{50}$: JCPDS File: 00-044-1433: d[Å] (I) | Co$_{50}$Fe$_{50}$: Experimental: d[Å] (I) | Fe: JCPDS File: 00-006-0696: d[Å] (I) |
|---|---|---|---|---|---|
| 1 | 1 1 0 | | 2.85700 super lattice | | |
| 2 | 1 1 1 | 2.04670 (100) | 1.64950 super lattice | | |
| 3 | 1 1 0 | | 2.02020 (100) | 2.01324 (100) | 2.02680 (100) |
| 4 | 2 0 0 | 1.77230 (40) | | 1.76957 (1.44) | |
| 5 | 2 0 0 | | 1.42850 (14) | 1.42690 (11) | 1.43320 (20) |
| 6 | 2 2 0 | 1.25320 (25) | | 1.25296 (0.97) | |
| 7 | 2 1 1 | | 1.16640 (25) | 1.16532 (20) | 1.17020 (30) |
| 8 | 3 1 1 | 1.06880 (30) | | 1.06804 (1.17) | |
| 9 | 2 2 2 | 1.02330 (12) | | | |
| 10 | 2 2 0 | | 1.01010 (8) | 1.00896 (5) | 1.01340 (10) |
| 11 | 3 1 0 | | 0.90350 (15) | 0.90270 (5) | 0.90640 (12) |
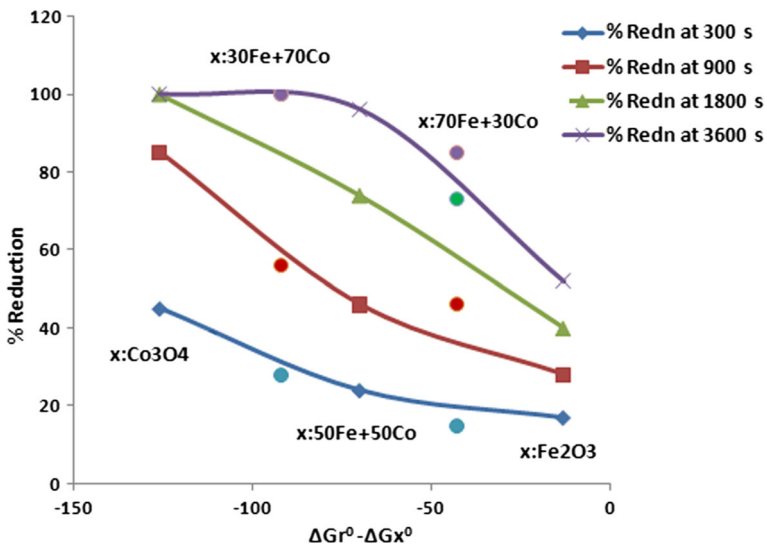


**Fig. 7** Extent of reduction (%) versus $\{(\Delta G_r^0) - \Delta G_x^0\}$. {x denotes $Fe_2O_3$, $Co_3O_4$ and ($Fe_2O_3 + Co_3O_4$)}. Microwave power: 750 W and hydrogen flow rate: $2.5 \times 10^{-6}$ m$^3$ s$^{-1}$

rose to 96% when cobalt oxide was added to the extent of 50% (Table 3, Fig. 5 and 7). Hydrogen utilization which was just 6.0% when iron oxide was reduced singularly rose to 10.33% during combined reduction. Cobalt oxide reduced alone results in 27.29% hydrogen utilization. This trend also corresponds to the free energy difference between the oxide and the reductant. A mention may be made that the $\{(\Delta G_r^0) - \Delta G_x^0\}$ value for $50Fe_2O_3$-$50Co_3O_4$ (−70 kJ/mol) is lower in magnitude than that for $50Fe_2O_3$-$50CuO$ (−125 kJ/mol). Yet, the improvement in reduction of iron oxide in the presence of cobalt oxide could be achieved, due to alloy formation of Fe and Co.

The XRD plots (Fig. 6) support the weight loss data presented in Table 3, Fig. 5 and Fig. 7. The plot for 3600 s reduction in Fig. 6 shows some unreduced materials mostly magnetite; not FeO which is conspicuously absent in all the three plots in Fig. 6 since it is not stable at lower temperatures. Thus hematite reduction here follows the sequence: $Fe_2O_3 \rightarrow Fe_3O_4 \rightarrow Fe$. As far as the peaks in Fig. 6 are concerned; Table 4 provides more detail information. It presents a comparison of XRD data (JCPDS Files) for Co, Fe metals as well as the $Co_{50}Fe_{50}$ alloy including the XRD pattern obtained from the product of this particular composition. Two factors are distinct in this table: the first one shows all the peaks of the alloy matching to those of the Fe metal, not Co; and the second is the slight increase in the 2θ position of the peaks in the alloy in comparison to the corresponding peak positions for Fe metal. The crystal size of the alloy calculated from this data is 2.8538 Å which is closer to 2.8670 Å, the crystal size of BCC Fe, rather than the crystal size of FCC Co metal which is 3.5447 Å. These observations are similar to those reported by Su et al. [11] which were interpreted as Co atoms placed in the lattice of Fe particles. Chon et al. [12] measured crystallite size of Fe–Co particles from the 110 reflections by using Scherrer's formula [$t = 0.9\lambda/\beta \cos\theta$] ($\lambda$ = X-ray wavelength and $\beta$ = FWHM). In a similar manner, the crystallite size of the Fe–Co product calculated from the present data for 3600 s experiment is 23 nm. Sundar et al. [10], referring to the binary Fe–Co diagram [13], have indicated that, at ambient temperatures, the inter-metallic compound FeCo ($\alpha'$) is stable in the range of 29–70 atomic % Co. This $\alpha'$ phase undergoes an order–disorder transformation when heated to a temperature above 1003 K. Under cooling below 773 K, B2 (CsCl), an ordered BCC structure of FeCo, can be achieved. They have also reported that the crystal size of the FeCo alloy decreases with increase in Co concentration.

## Variation in the Proportion of Iron Oxide and Cobalt Oxide

Keeping in view the stability of the Fe–Co inter-metallic compound in the range of 29–70 atomic % Co [10], two more sets of reduction experiments were conducted with mixtures of $Co_3O_4$ and $Fe_2O_3$ in two proportions, such that the resultant product when totally reduced would be metallic Co-Fe in the following ratios: (30:70) and (70:30). The microwave power of 750 W and hydrogen flow rate of $2.5 \times 10^{-6}$ $m^3$ $s^{-1}$ was maintained all through the experiments. The results of weight loss at various time periods along with pressure and temperature data are reported in Table 5. The reduction rate plots are presented as (b) and (d) in Fig. 5, and the XRD results in Fig. 8 and Table 6. The extent of reduction (%) versus $\{(\Delta G_r^0) - \Delta G_x^0\}$ plots for these two specific proportions are also included in Fig. 7 as bold points under (x = 70Fe + 30Co) and (x = 30Fe + 70Co). Here also Fig. 8, as well as Table 6, shows the Fe–Co alloy to be the dominant product. Therefore, as in Sect. 3.2, higher levels of reduction for iron oxide have also been achieved when cobalt oxide is added to iron oxide. The reduction (together) rose to 84 and ~100% (~100% even by 1800 s) in 3600 s when cobalt oxide was added to the extent of 30 and 70% (by weight), respectively (Table 5, Figs. 5 and 7). Hydrogen utilization also rose to 9.48 and 20.86% during combined reduction with 30 and 70% cobalt oxide, respectively. The XRD plots (Fig. 8) support the weight loss data presented in Table 5, Figs. 5 and 7. The plot for 3600 s reduction in Fig. 8a (30Co–70Fe) shows some small peaks of magnetite left unreduced because of higher iron oxide content. These peaks are very few in Fig. 8b (70Co–30Fe), where the proportion of iron oxide is low. However, because of higher Co to Fe ratio, all the reduced Co metal did not form Fe–Co alloy, and some peaks for Co metal are visible in Fig. 8b. The 1800 s reduction plot for this composition, though not shown here, has attained the level of reduction similar to that at 3600 s, meaning the reduction is

**Table 5** Weight loss as well as maximum pressure and temperature for reduction of $Fe_2O_3$, ($Co_3O_4$ + $Fe_2O_3$) and $Co_3O_4$ at various proportions with hydrogen plasma. Microwave power: 750 W and hydrogen flow rate: $2.5 \times 10^{-6}$ $m^3$ $s^{-1}$

| Raw material | Time/ s | $T_{max}$,/ K | $P_{max}$,/ $10^2$ Pa | Initial wt/ $10^{-3}$ kg | Final wt/ $10^{-3}$ kg | Wt loss,/ $10^{-3}$ kg | Reduction, in % |
|---|---|---|---|---|---|---|---|
| 70Fe-30Co | 300 | 742.1 | 1.624 | 2.527 | 2.417 | 0.109 | 15 |
| 70Fe-30Co | 600 | 811.4 | 1.808 | 2.548 | 2.287 | 0.260 | 36.1 |
| 70Fe-30Co | 900 | 841.2 | 1.757 | 2.547 | 2.216 | 0.331 | 45.9 |
| 70Fe-30Co | 1800 | 839.4 | 1.724 | 2.548 | 2.022 | 0.526 | 72.9 |
| 70Fe-30Co | 2700 | 828.2 | 1.816 | 2.556 | 1.987 | 0.573 | 79.3 |
| 70Fe-30Co | 3600 | 794.6 | 1.783 | 2.544 | 1.934 | 0.609 | 84.6 |
| 30Fe-70Co | 300 | 751.4 | 1.900 | 2.555 | 2.370 | 0.185 | 28,2 |
| 30Fe-70Co | 600 | 738.4 | 1.808 | 2.537 | 2.255 | 0.282 | 43.5 |
| 30Fe-70Co | 1200 | 737.6 | 1.824 | 2.498 | 2.050 | 0.448 | 69.2 |
| 30Fe-70Co | 1500 | 828.5 | 1.724 | 2.45 | 1.936 | 0.513 | 81.2 |
| 30Fe-70Co | 1800 | 834.2 | 1.957 | 2.538 | 1.868 | 0.670 | 102.4 |
| 30Fe-70Co | 3600 | 784.9 | 1.849 | 2.544 | 1.875 | 0.668 | 101.3 |

near complete even by 1800 s because of the presence of higher cobalt oxide and lower iron oxide. In these two series of experiments also FeO is absent meaning $Fe_2O_3 \rightarrow Fe_3O_4 \rightarrow Fe$ is the sequence of reduction of hematite.

Table 6 presents a detailed analysis of the XRD peaks obtained for all the three (70Fe–30Co, 30Fe–70Co, and 50Fe–50Co of the earlier section) FeCo alloy compositions. The peak positions match to peaks of the corresponding Fe–Co alloy composition as per the JCPDS Files mentioned therein. The last-but-one row in the table provides the lattice parameters calculated from these data which are 2.8663, 2.8538 and 2.8374 Å for FeCo alloys containing 30, 50 and 70% Co, respectively. The lattice parameters show a decreasing trend with the increase in Co content in the alloy similar to that reported by Sundar et al. [10]. Similarly, the last row presents the crystallite size calculated using Scherrer's formula for the product obtained in the experiments of 3600 s duration. These values are 30, 23, and 22 nm, for FeCo alloys containing 30, 50 and 70% Co, respectively. Further, Sourmail [9] has reported that the order parameter can be related to the ratio $I_{\{100\}}$/$I_{\{200\}}$ where $I_{\{hkl\}}$ is the intensity of the line of corresponding indices in the super-lattice. Chon et al. [12] used this principle to evaluate ordering/disordering taking {100} and {111} indices. In an identical manner, using the d values for {100} and {111} indices from Table 4, the XRD plots of the products obtained after 3600 s reduction in the present study were expanded to observe the narrow ranges where {100} (d = 2.85700 Å) and {111}
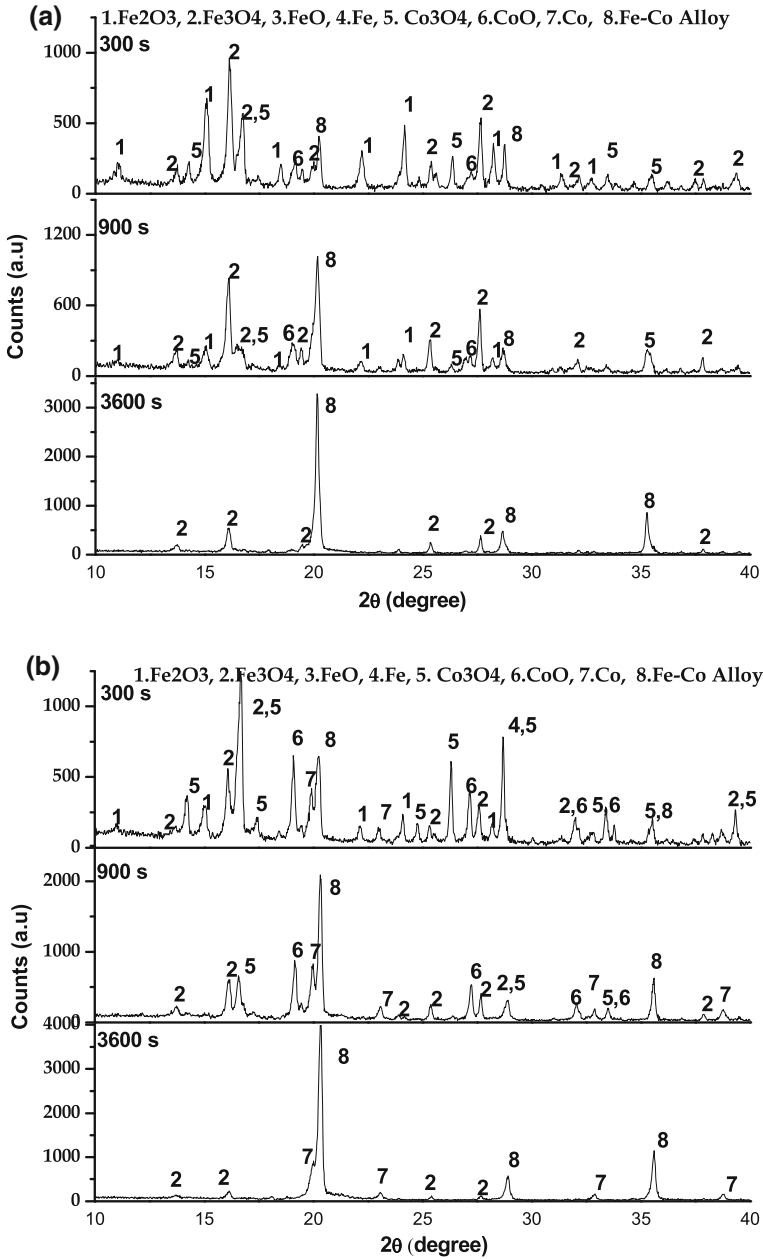
**Fig. 8** XRD plots for reduction of $Fe_2O_3 + Co_3O_4$ which would result in **a** 70–30, **b** 30–70 Fe–Co metal. Microwave power: 750 W and hydrogen flow rate: $2.5 \times 10^{-6}$ m$^3$ s$^{-1}$, time: 3600 s

(d = 1.64950 Å) indices occur and no diffraction peaks were detected. Thus a same conclusion made here that the FeCo products obtained in the present study have a disordered structure. The maximum temperature attained in these experiments is 860 K (Tables 3 and 5) which is much less than 1003 K, the temperature above which the material

**Table 6** XRD data obtained from the product after reduction of (Fe$_2$O$_3$ + Co$_3$O$_4$) with hydrogen plasma for 3600 s. Microwave power: 750 W and hydrogen flow rate: $2.5 \times 10^{-6}$ m$^3$ s$^{-1}$

| Serial No. | Plane h k l | Co$_{30}$Fe$_{70}$: JCPDSFile: 48-1816: d[Å] (I) | Co$_{30}$Fe$_{70}$: Experimental: d[Å] (I) | Co$_{50}$Fe$_{50}$: JCPDSFile: 44-1433: d[Å] (I) | Co$_{50}$Fe$_{50}$: Experimental: d[Å] (I) | Co$_{70}$Fe$_{30}$: JCPDSFile: 50-0795: d[Å] (I) | Co$_{70}$Fe$_{30}$: Experimental: d[Å] (I) |
|---|---|---|---|---|---|---|---|
| 1 | Co 1 1 1 | | | | | | 2.0501 (17.74) |
| 2 | Fe-Co 1 1 0 | 2.0035 (100) | 2.0257 (100) | 2.0202 (100) | 2.0132 (100) | 2.0057 (100) | 2.0101 (100) |
| 3 | Co 2 0 0 | | 1.7746 (0.77) | | 1.7696 (1.44) | | 1.7759 (3.11) |
| 4 | Fe-Co 2 0 0 | 1.4315 (10) | 1.4331(12) | 1.4285 (14) | 1.4269 (11) | 1.4198 (9) | 1.4187 (11) |
| 5 | Co 2 2 0 | | | | 1.2530 (0.97) | | 1.2529 (2.82) |
| 6 | Fe-Co 2 1 1 | 1.1689 (37) | 1.1699 (23) | 1.1664 (25) | 1.1653 (20) | 1.1596 (33) | 1.1599 (3) |
| 7 | Co 3 1 1 | | 1.0687 (0.78) | | 1.0680 (1.17) | | 1.0683 (2.62) |
| 8 | Fe-Co 2 2 0 | 1.0125 (14) | 1.0130 (6) | 1.0101 (8) | 1.0090 (5) | 1.0044 (8) | 1.0045 (5) |
| 9 | Fe-Co 3 1 0 | | 0.9065 (5) | 0.9035 (15) | 0.9027 (5) | | |
| Crystal size | | 2.8634 Å | 2.8663 Å | 2.8570 Å | 2.8538 Å | 2.8403 Å | 2.8374 Å |
| Crystallite size | | | 30 nm | | 23 nm | | 22 nm |

is to be heated so as to have the ordered transformation during cooling. It may be the reason for not having an ordered structure.

## Reaction Mechanism

Two processes are occurring here: the first is the conversion of hydrogen gas into the plasma state and the second is the reduction of oxides. The mechanism of reduction of oxides of iron [2, 3], copper [6] and cobalt [5] has already been discussed earlier. In the present case, Fe and Cu have been shown to be reduced independently; thus, the mechanism of reduction of each one might be as discussed earlier. Figures 2 and 3 are showing near completion of reduction of copper oxide by 1200 s, whereas, iron metal formation builds up subsequently. Thus the plots (a) for $Fe_2O_3$ and (c) the mixture of $Fe_2O_3$ and CuO in Fig. 2 run almost parallel after 900 s which is indicative of the reduction of iron oxide to Fe during this period. Interestingly, no peak for FeO is visible in Fig. 3 for 3600 s product; may be due to the fact that the maximum temperature achieved (746.2 K) in the case of 3600 s experiment is less than 841 K above which FeO is stable. This situation shows a smooth reduction of magnetite directly to Fe metal without any kinetic hindrance because of the presence of plasma. In the case of the other products at 360 and 1200 s in Fig. 3, just a couple of FeO peaks are visible because the maximum temperatures achieved in those cases are slightly higher.

In the case of the other combination, Fe and Co have formed their alloy. In this case, also, the relative intensities of cobalt oxide and iron oxide peaks indicate that reduction of cobalt oxide precedes that of iron oxide. It is seen that most of the cobalt oxide has been reduced to the metallic state by 1200 s by which time only a small portion of iron oxide has been reduced to Fe metal. Further, the relative intensities of FeCo peaks are predominant in comparison to that of Co metal peaks which indicate that FeCo formation is preferred in these conditions. Some Co remains as FCC Co only in case of (70Co + 30Fe). Reduction of iron oxide is less than total by 3600 s in the case of 70Fe–30Co and 50Fe–50 Co, whereas, it is complete by even 1800 s in the case of 30Fe–70Co. Since, FeCo form alloy of the same phase in a wide range of compositions [10], and the temperature conditions prevail throughout the reduction period, alloy formation with homogenization may not face any problem. Probably in earlier periods, the FeCo formed might be rich in cobalt, and more and more iron metal might have continued to enter into the alloy phase after reduction through diffusion and homogenization.

Some observations are listed in Table 7 in the form of intensities of particular peaks representing Co metal at 1200 s and 3600 s reduction, as well as the crystal lattice strain

**Table 7** Intensities (I) of various Co peaks along with that of the FeCo (110) peak obtained from XRD data for the products after reduction of ($Fe_2O_3$ + $Co_3O_4$) of various composition and time with hydrogen plasma. Microwave power: 750 W and hydrogen flow rate: $2.5 \times 10^{-6}$ m$^3$ s$^{-1}$

| Fe: Co | Time, s | I, Co(111) | I, Co(200) | I, Co(220) | I, Co(311) | I, FeCo | Latt. Str. % |
|--------|---------|-----------|-----------|-----------|-----------|---------|--------------|
| 30:70  | 1200    | 34.25     | 8.70      | 6.10      | 5.88      | 100     | 0.13         |
| 30:70  | 1800    | 17.15     | 3.66      | 2.61      | 2.16      | 100     | 0.28         |
| 30:70  | 3600    | 17.74     | 3.11      | 2.82      | 2.62      | 100     | 0.28         |
| 50:50  | 1200    | –         | 3.54      | 3.30      | 3.01      | 100     | 0.28         |
| 50:50  | 3600    | –         | 1.44      | 0.97      | 1.17      | 100     | 0.26         |
| 70:30  | 1200    | –         | 3.44      | –         | –         | 100     | 0.18         |
| 70:30  | 3600    | –         | 0.77      | –         | 0.78      | 100     | Reference    |

estimated from the broadening of Fe–Co (110) peak for all the three Fe–Co alloys. First of all, the peaks of Co metal become increasingly prominent with the rise in Co content in the alloy. Further, those are more prominent in the samples obtained after 1200 s reduction in comparison to that obtained after 3600 s reduction. This means cobalt metal is forming earlier than iron metal, gets into the alloy system subsequently when Fe forms. Thus the peak intensity of Co in the 1200 s product is higher than that in the 3600 s product.

The broadening of the peak (FWHM) can also be used for estimating lattice strain [14–16] which is a feature in case of alloy formation. The formula here is: $[\varepsilon = (\beta_r/4\tan\theta)]$, where, $\varepsilon$ = lattice strain, $\beta$ is FWHM and $\theta$ is the angle. Usually, $\beta$ is obtained by eliminating the broadening due to the instrument from that measured following the formula: $[\beta = \sqrt{\{(\beta_{\text{measured}})^2 - (\beta_{\text{due to the instrument}})^2\}}]$; and ($\beta_{\text{due to the instrument}}$) is determined using a well-annealed sample. In the present case the sample (70% Fe and 30% Co) where the lowest cobalt is present and the strain is expected to be minimum (in fact, the observed FWHM is minimum) has been taken as ($\beta_{\text{due to the instrument}}$) for calculating the lattice strain. The strain estimated in this manner may not represent the real strain, yet, it may be taken as a relative value for comparison purpose. These values are presented in Table 7, last column as the percentage and indicate that in the case of the alloy with (70% Fe and 30% Co), the strain is 0.18% at 1200 s stage when metallic Fe formation is quite less. This strain is relieved by 3600 s with the appearance of more Fe. Similarly, in the case of (50% Fe and 50% Co), there is 0.28% strain at 1200 s which is slightly relieved to 0.26% by 3600 s with the appearance of more Fe. In the case of (30% Fe and 70% Co), the situation is different. Here, the availability of Fe is less, and that of cobalt is abundant, and therefore, probably Fe is forming and diffusing into the lattice causing strain, and thus, the strain is 0.13% at 1200 s instant which is growing to 0.28% by 1800 s and remains same for 3600 s. Since the highest temperature is below 873 K (Tables 3 and 5), and the cooling is slow furnace cooling, the alloy formed is disordered [12].

In the case of conversion of hydrogen to the plasma state, a mention about average microwave power density (MWPD) and its effect on the reduction process in low-temperature plasma systems is warranted [17, 18]. In the present study, the pressure and temperature reported in Tables 1, 3 and 5 fell within a narrow range of 1467–3067 Pa and 595–860 K, respectively. The estimated MWPD was within a narrow range of $4 \times 10^6$–$9 \times 10^6$ W m$^{-3}$. This case is also similar to the earlier cases [5, 6]. Therefore, the expected mole fraction of atomic hydrogen should be in the range of 0.01–0.02 [18] and the dominant hydrogen species may be vibrationally excited hydrogen molecules. The plasma (gas) would transfer energy as well as the reductant species while interacting with the oxide substrate [1]. The vibrationally excited H$_2$ molecules ($\upsilon = 0$–4), stronger reductants than molecular hydrogen are expected to play an important role in the reduction process. The rate of emergence of vibrationally excited hydrogen species from the plasma and appearance at the oxides plasma interface may be significant.

## Conclusions

During reduction of oxide mixtures of Fe and Cu, each oxide was reduced independently forming a mechanical mixture of Cu and Fe metals. Enhancement in the reduction of iron oxide was marginal. In contrast to (Fe$_2$O$_3$ + CuO), reduction of oxide mixtures of Fe and Co led to the formation of FeCo alloy. This alloy formation was extensive within a Co concentration of 30–70%, and the crystal size decreased with increase in Co concentration.

Iron reduction followed the sequence of $Fe_2O_3 \rightarrow Fe_3O_4 \rightarrow Fe$; no FeO formed since the temperature was lower than 841 K above which FeO is stable. Because of lower temperature, solid oxide—plasma interaction took place which resulted in Fe–Co powder in the range of 22–30 nm. Again due to a lower temperature (less than 1003 K) the alloy formed had a disordered structure. Reduction of $Co_3O_4$ was relatively faster than that of $Fe_2O_3$. Hence, alloy formation was taking place with higher lattice strain during the earlier period of reduction, and the lattice strain got reduced with time with the formation of more metallic Fe. At higher Co content (70% Co), all the Co did not get accommodated in the alloy and part of it remained in the metallic state. The average microwave power density which is a critical parameter that influences the reduction process through regulation of excited species in hydrogen plasma was also estimated.

# References

1. Sabat KC, Rajput P, Paramguru RK, Bhoi B, Mishra BK (2014) Plasma Chem Plasma Process 34(1):1–23
2. Rajput P, Bhoi B, Sahoo S, Paramguru RK, Mishra BK (2013) Ironmak Steelmak 40(1):61–68
3. Rajput P, Sabat KC, Paramguru RK, Bhoi B, Mishra BK (2014) Ironmak Steelmak 41(10):721–731
4. Bhoi B, Mishra BK, Paramguru RK, Pradhan SK, Mukherjee PS, Sahoo S, Das SK (2014) US Pat 8728195
5. Sabat KC, Paramguru RK, Pradhan S, Mishra BK (2015) Plasma Chem Plasma Process 35:387–399
6. Sabat KC, Paramguru RK, Mishra BK (2016) Plasma Chem Plasma Process 36(4):1111–1124
7. Sundar MS, Klaua M, Shen J, Barthel J, Jenniches H, Kirschner J (1998) Phys Rev B 58(13):8549–8555
8. Lucas FM, Trindade B, Costa BFO, Le Caer G (2002) Key Eng Mater 230–232:631–634
9. Sourmail T (2005) Prog Mater Sci 50(7):816–880
10. Sundar RS, Deevi SC (2005) Int Mater Rev 50(3):157–192
11. Xiaobo Su, Huagui Zheng, Zhiping Yang, Yongchun Zhu, Anlian Pan (2003) J Mater Sci 38:4581–4585
12. Chon GB, Shinoda K, Suzuki S, Jayadevan B (2010) Mater Trans 51(4):707–711
13. Nishizawa T, Ishida K (1990) In: Massalski TB (ed) Binary alloy phase diagrams, vol 2. Metals Park, New York
14. Bindu P, Thomas S (2014) J Theor Appl Phys 8(4):123–134
15. Suryanarayana C, Norton MG (1998) X-ray diffraction a practical approach. Plenum Press, New York
16. Cullity BD, Stock SR (2001) Elements of X-ray diffraction, 3rd edn. Prentice-Hall, New York
17. Hassouni K, Gicquel A, Capitelli M, Loureiro J (1999) Plasma Sour Sci Technol 8(3):494
18. Hassouni K, Grotjohn TA, Gicquel A (1999) J Appl Phys 86(1):134–151